This is a preprint, the final version is subject to change, of the American Mineralogist (MSA)
Cite as Authors (Year) Title. American Mineralogist, in press.
DOI: https://doi.org/10.2138/am-2020-7311

Revision 1

The new K, Pb-bearing uranyl-oxide mineral kroupaite: crystal-chemical implications for the structures of uranyl-oxide hydroxy-hydrates

JAKUB PLÁŠIL[1§], ANTHONY R. KAMPF[2], TRAVIS A. OLDS[3], JIŘÍ SEJKORA[4], RADEK ŠKODA[5], PETER C. BURNS[3] AND JIŘÍ ČEJKA[4]

[1] Institute of Physics ASCR, v.v.i., Na Slovance 1999/2, 18221 Prague 8, Czech Republic
[2] Mineral Sciences Department, Natural History Museum of Los Angeles County, 900 Exposition Boulevard, Los Angeles, CA 90007, USA
[3] Department of Civil and Environmental Engineering and Earth Sciences, University of Notre Dame, Notre Dame, IN 46556, USA
[4] Department of Mineralogy and Petrology, National Museum, Cirkusová 1740, Prague 9 - Horní Počernice, 193 00, Czech Republic
[5] Department of Geological Sciences, Faculty of Science, Masaryk University, Kotlářská 2, 611 37, Brno, Czech Republic

ABSTRACT

Kroupaite (IMA2017-031), ideally $KPb_{0.5}[(UO_2)_8O_4(OH)_{10}]\cdot 10H_2O$, is a new uranyl-oxide hydroxyl-hydrate mineral found underground in the Svornost mine, Jáchymov, Czechia. Electron-probe microanalysis (WDS) provided the empirical formula $(K_{1.28}Na_{0.07})_{\Sigma 1.35}(Pb_{0.23}Cu_{0.14}Ca_{0.05}Bi_{0.03}Co_{0.02}Al_{0.01})_{\Sigma 0.48}[(UO_2)_{7.90}(SO_4)_{0.04}O_{4.04}(OH)_{10.00}]\cdot 10H_2O$, basis of 40 O atoms apfu. Sheets in the crystal structure of kroupaite adopt the fourmarierite anion topology, and therefore kroupaite belongs to the schoepite-family of minerals with related structures differing in the interlayer composition and arrangement, and charge of the sheets. Uptake of dangerous radionuclides (^{90}Sr oir ^{135}Cs) into the structure of kroupaite and other

§ Email: plasil@fzu.cz

Always consult and cite the final, published document. See http:/www.minsocam.org or GeoscienceWorld

uranyl-oxide hydroxy-hydrate is evaluated based on crystal-chemical considerations and Voronoi-Dirichlet polyhedra measures. These calculations show the importancy of these phases for the safe disposal of nuclear waste.

Keywords: kroupaite; new mineral species; uranyl-oxide hydroxy-hydrate; crystal structure; Voronoi-Dirichlet polyhedra; ^{135}Cs; ^{90}Sr; Jáchymov.

INTRODUCTION

Uranium dioxide, as nuclear fuel or uraninite (Janeczek et al. 1996), UO_{2+x}, readily reacts with oxygen and water to form a fascinating family of uranyl-oxide hydroxyl-hydrates (UOHs) (Finch and Ewing 1992; Wronkiewicz et al. 1996; Plášil 2014). These occur in nature as minerals and are amongst the first alteration products that form during weathering of uraninite in oxidized zones of U deposit worldwide (Finch et al. 1996a, b; Plášil 2018a). They are of interest in forensics studies of intercepted illicit nuclear materials as they provide insights into uranium oxide history. Number of studies has focused on their structure, solubility, and thermodynamic stability (Casas et al. 1997; Finch and Murakami 1999; Klingensmith et al. 2007; Kubatko et al. 2006a; Gorman-Lewis et al. 2008; Kirkegaard et al. 2019). It is due to their general importance in nuclear waste disposal and the environmental chemistry of uranium.

The onset of oxidation and hydration of uranium oxide often yields phases consisting of electroneutral sheets of uranyl pentagonal bipyramids with substantial H_2O in the interlayer region, and typically little, if any, additional metal cations (Burns 2005; Krivovichev and Plášil 2013; Lussier et al. 2016; Plášil 2018a). In some cases, uranium oxide hydrates containing mixtures of U(IV), U(V) or U(VI) oxidation states occur as well. Continued alteration of uranium

Always consult and cite the final, published document. See http:/www.minsocam.org or GeoscienceWorld

oxide, alteration in more chemically diverse aqueous fluids, and alteration of geologically old uranium oxide that contains substantial radiogenic lead leads to formation of uranyl-oxide hydroxy-hydrates with anionic sheets of uranyl polyhedra charge-balanced by cations in the interstitial regions of the structures.

Here we describe the new mineral kroupaite that was found underground in the Svornost (formerly "Einigkeit" in German) mine in Jáchymov, Western Bohemia, Czechia. Details of the mineralogy, geology and history of the Jáchymov ore district can be found elsewhere (Ondruš et al. 2003; Hloušek et al. 2014). The specimens studied originate from the Jan Evangelista vein at the Daniel level of the Svornost mine. Associated minerals include fourmarierite, Na-rich metaschoepite, uranopilite, liebigite, ewingite and gypsum. The new mineral and its assemblage are of supergene origin associated with oxidation-hydration alteration of uraninite in old mine workings. The name honors mining engineer Gustav Kroupa (1857–1935), who was employed by the state mines in Jáchymov beginning in 1886, and who as head of the mining district, approved shipment of 10 tons of leachate obtained from processing pitchblende ore to Marie-Curie Sklodowska and Pierre Curie in 1898. They went on to isolate three grams of the new substance radium chloride, and subsequently the new element radium. The Commission on New Minerals, Nomenclature and Classification of the International Mineralogical Association approved the new mineral and name (IMA2017-031). The description is based upon the holotype specimen deposited in the mineralogical collection of the National Museum in Prague (catalogue number no. P1P 16/2017). Crystals used in this study are deposited in the Natural History Museum of Los Angeles County (catalogue number 66572).

PHYSICAL AND OPTICAL PROPERTIES

Always consult and cite the final, published document. See http:/www.minsocam.org or GeoscienceWorld

Kroupaite forms as radial aggregates of thick platy, orange-yellow crystals up to 1 mm in diameter (Fig. 1) growing in interstices of gypsum crystals. Tablets are flattened on {100}, with the prominent crystal forms {100}, {013} and {021} (Fig. 2). Crystals are brittle with at least one perfect cleavage on {100} and uneven fracture. Crystals are translucent with vitreous luster, have light yellow streak, and are non-fluorescent under LW and SW ultraviolet radiation. The Mohs hardness is approximately 2, estimated by scratch tests . The density was not measured due to the limited availability of material. The calculated density is 5.058 g/cm^3 based on the empirical formula. Kroupaite is readily soluble in dilute HCl, with no effervescence.

Kroupaite is optically biaxial (–), with $\alpha = 1.691(2)$, $\beta = 1.752(2)$, $\gamma = 1.768(2)$ (measured with white light). The $2V$ is 53(1)°, measured directly by conoscopic observation on a spindle stage; the calculated $2V$ is 52.7°. Dispersion is strong, $r > v$. The mineral is pleochroic with X colorless, Y yellow and Z yellow; $X < Y \approx Z$. The optical orientation is $X =$ **a**, $Y =$ **c**, $Z =$ **b**. The Gladstone-Dale compatibility (Mandarino 2007), $1 - (K_p/K_c)$, is –0.018 (superior) for the empirical formula.

RAMAN SPECTROSCOPY

A Raman spectrum was collected in the range 4500–12 cm^{-1} using a DXR dispersive Raman Spectrometer (Thermo Scientific) mounted on a confocal Olympus microscope. The Raman signal was excited by a green 532 nm diode-pumped solid-state laser and was collected by a CCD detector. The experimental parameters were: 50× objective, 10 s exposure time, 100 exposures, 400 lines/mm grating, 50 μm pinhole spectrograph aperture and 1 mW laser power level. The instrument was set up by a software-controlled calibration procedure using multiple neon emission lines (wavelength calibration), multiple polystyrene Raman bands (laser frequency

Always consult and cite the final, published document. See http:/www.minsocam.org or GeoscienceWorld

calibration) and standardized white-light sources (intensity calibration). Spectral manipulations as well as band-fitting were performed using the Omnic 9 software (Thermo Scientific).

In the Raman spectrum of kroupaite (Fig. 3a) a weak broad band at 3487 cm^{-1} is assigned to the ν O–H stretching vibrations of hydroxyl and molecular H_2O H-bonded into the structure. The approximate bond-lengths of H-bonds (H···*Acceptor*) lie in the range 1.8–2.0 Å (Libowitzky 1999). The strong band centered at 833 cm^{-1}, with a shoulder at 812 cm^{-1} (Figure 3b), is attributed to the ν_1 symmetric stretching vibration of uranyl U–O. The splitting of the ν_1 of $(UO_2)^{2+}$ is concomitant with four unique U sites observed in the crystal structure. Based on recent theoretical and experimental studies (Colmenero et al. 2018; Kirkegaard et al. 2019), the assignment of the vibration bands directly to ν_1 $(UO_2)^{2+}$ is not straightforward: the component bands comprise both symmetric stretching ν_1 $(UO_2)^{2+}$ and δ (U–OH), as well as libration vibration of (H_2O). Nevertheless, using an empirical relationship to derive the approximate U–O bond lengths from the band positions assigned to the $(UO_2)^{2+}$ stretching vibrations gives ~1.78 Å (833 cm^{-1}) and ~1.80 Å (812 cm^{-1}) (Fig. 3b). These values are in line with U–O bond-lengths obtained from the crystal structure data (see Table 2). There is a series of weak bands in the 580–280 cm^{-1} range (570, 542, 500, 450, 400, 328, 298 cm^{-1}). Those at 570–500 cm^{-1} are attributable to librations of H_2O. Those at 450–328 cm^{-1} can be assigned to δ ($O–U–O_{eq}$) vibrations. According to a theoretical study of schoepite (Colemenero et al. 2018, 2019), these bands also have a significant contribution of the ν ($U–O_{eq}$), δ (U–OH) and libration of H_2O. The band at 298 cm^{-1} is attributed to ν_2 (δ) $(UO_2)^{2+}$, but there may be contributions from δ ($O–U–O_{eq}$), δ (U–OH) and water librations. Remaining bands located below 200 cm^{-1} (190, 155, 116, 63, 40 cm^{-1}) are assigned to molecular deformations and lattice modes.

Always consult and cite the final, published document. See http:/www.minsocam.org or GeoscienceWorld

CHEMICAL ANALYSIS

Kroupaite was analyzed by electron microprobe using a Cameca SX100 electron microprobe (Masaryk University, Brno) operating in wavelength dispersive spectroscopy mode using an accelerating voltage of 15 kV, beam current of 4 nA and a 10–15 μm beam diameter. Concentrations of elements other than those reported in Table S1 were below detection limits (ca 0.03–0.10 wt. %). The low analytical totals are due to an uneven surface and the porosity of the polished section; therefore, we also report normalized data (column "Norm." in Table 1). A matrix correction was applied to the data using the '*PAP*' software (Pouchou and Pichoir 1991). The H_2O content was calculated by stoichiometry (obtained from the structure); the paucity of pure material precluded a direct determination of the H_2O content. The empirical formula calculated on the basis of 40 O atoms per formula unit is: $(K_{1.28}Na_{0.07})_{\Sigma 1.35}(Pb_{0.23}Cu_{0.14}Ca_{0.05}Bi_{0.03}Co_{0.02}Al_{0.01})_{\Sigma 0.48}[(UO_2)_{7.90}(SO_4)_{0.04}O_{4.04}(OH)_{10.00}]\cdot 10H_2O$. The ideal formula is $KPb_{0.5}[(UO_2)_8O_4(OH)_{10}]\cdot 10H_2O$, which requires: K_2O 1.73, PbO 4.11, UO_3 84.21, H_2O 9.95, total 100 wt%.

X-RAY CRYSTALLOGRAPHY AND STRUCTURE DETERMINATION

Powder diffraction data were collected using a Rigaku R-Axis Rapid II curved imaging plate microdiffractometer with monochromated MoK_α radiation. A Gandolfi-like motion on the φ and ω axes was used to randomize the sample. Observed *d*-values and intensities were derived by profile fitting using the JADE 2010 software (Materials Data, Inc.). Data are given in Table 2. Unit-cell parameters refined from the powder data using JADE 2010 with whole pattern fitting are: a = 14.781(7) Å, b = 14.095(6) Å, c = 16.719(7) Å, V = 3583(3) Å^3, Z = 4 (space group: *Pbca*).

Always consult and cite the final, published document. See http:/www.minsocam.org or GeoscienceWorld

Single-crystal X-ray diffraction data were collected at room temperature on a Rigaku SuperNova diffractometer equipped with a microfocus X-ray source (MoK_α, $\lambda = 0.71073$ Å) and an Atlas S2 CCD detector. The crystal, 0.07 × 0.06 × 0.03 mm large, was mounted on a cut microloop. The raw data reduction was done using CrysAlis software (Rigaku 2019). An absorption correction combining a Gaussian correction and an empirical scaling was applied to the data using the Jana2006 software (Petříček et al. 2014). The structure was solved with SHELXT using charge-flipping (Sheldrick 2015). Full-matrix least squares refinement of the structure against F^2 was performed with Jana2006 (Petříček et al. 2014); the structure has been refined to R = 0.0447 for 2587 unique observed reflection. The crystallographic data can be found in the original cif file (as supplementary file); selected interatomic distances and results of the bond-valence analysis are given in Tables 3 and 4, respectively..

DESCRIPTION OF THE STRUCTURE

Kroupaite crystallizes in orthorhombic space group *Pbca* and its structure (Fig. 4) contains four U sites, one K site, one Pb site and nineteen O sites. Each U site is coordinated by seven ligands (Table 3), forming pentagonal bipyramids, where the apices of each bipyramid are comprised of strongly bonded O atoms, forming the approximately linear uranyl ion, UO_2^{2+}. In the equatorial plane, each uranyl ion is bonded to five ligands, either O or OH^- (Table 4), and the polyhedra polymerize by sharing edges and equatorial vertices (Fig. 4) into the well-known fourmarierite anion sheet topology (Fig. 5) (Burns 2005; Krivovichev and Plášil 2013; Lussier et al. 2016). In the interlayer, there are two independent cation sites that are occupied by K^+ and Pb^{2+}. Both sites have occupancies lower than unity. Additionally, there are four O sites (O15, O16, O18, O19) in the interlayer corresponding to H_2O molecules (Table 4) that were identified

Always consult and cite the final, published document. See http:/www.minsocam.org or GeoscienceWorld

based on the bond-valence sums incident upon the corresponding O atoms. The K atom is [7]-fold coordinated (to 3.3 Å) and binds to five distinct O_{Ur} (*Ur* – uranyl) atoms. Site-scattering refinement revealed that the site is partially occupied (~0.47/0.5). The Pb site is [9]-fold coordinated (to 3.3 Å); six of the ligands are O_{Ur} atoms from adjacent structural sheets, with three from each sheet, and thus the Pb cations directly bridge between sheets. There are dimers of Pb polyhedra; one Pb-polyhedron is linked to its symmetrical equivalent through the pair of symmetrically related O16(H_2O) atoms to form $Pb_2O(O_{Ur})_{10}(H_2O)_3$ dimers.

According to the bond-valence analysis and site-scattering refinement the formula, assuming full metal-cation site occupancy for K (0.94 K from the site-scattering refinement) and 0.5 Pb (0.44 from refinement) and full occupancies of the O(H_2O) sites, is $KPb_{0.5}[(UO_2)_8O_4(OH)_{10}]\cdot 8H_2O$, $Z = 4$, although the H_2O content is likely somewhat lower.

RELATIONSHIP TO OTHER UOH MINERALS AND COMPOUNDS

The structural unit in kroupaite is the well-known fourmarierite-type sheet, which accommodates various combinations of OH^- and O in uranyl minerals, and thus has variable charge. Electroneutral sheets with composition $[(UO_2)_4O(OH)_6]$ occur in schoepite and metaschoepite (Plášil 2018b; Weller et al. 2000), whereas anionic sheets with composition $[(UO_2)_4O_2(OH)_5]^-$ occur in synthetic Na-bearing metaschoepite (Klingensmith et al. 2007) and leesite (Olds et al. 2018), and with composition $[(UO_2)_4O_3(OH)_4]^{2-}$ in fourmarierite (Li and Burns 2000a).

Lead cations in the structure of kroupaite occupy the same site as Pb^{2+} in fourmarierite, but surprisingly, also the same site as K^+ in leesite (Fig. 5). In the structure of kroupaite, K atoms occupy the site adjacent to the dimeric Pb polyhedral units. The different behaviors of K and Pb

Always consult and cite the final, published document. See http:/www.minsocam.org or GeoscienceWorld

in the structures of kroupaite and leesite are well documented by distinct substitution trends between kroupaite and fourmarierite (characteristic for the same Pb sites) and leesite (Fig. 6). The substitution in leesite should take place at the single cationic site for Pb^{2+} and K^{+}. The main structural distinction of kroupaite from leesite is a unique K^{+} site in kroupaite (Fig. 5). It appears that in the presence of Pb^{2+} with a stereoactive lone pair of electrons, K^{+} is favored at a site that provides more space and, consequently, K atoms shift to a position beneath bounding O_{Ur} atoms. The corresponding Voronoi-Dirichlet polyhedral values that characterize particular coordination environments of metal cations in the interlayers of kroupaite, leesite, fourmarierite (Fig. 7) and synthetic Na-metaschoepite are given in Table 5. Comparing Lewis acid (LA) strengths, Pb^{2+} is a much stronger acid (0.22 *vu*) than K^{+} (0.11 *vu*). Both kroupaite and leesite contain similar amounts of H_2O in their interlayers (kroupaite is slightly more hydrated) and the arrangement of $(OH)^{-}$ in the kroupaite sheet is identical to that found both in leesite and synthetic Na-metaschoepite. The consequence is that Pb adopts a site in the kroupaite structure that is more compatible with the distribution of higher bond-valence from Lewis acids to Lewis bases; in kroupaite the average Pb^{2+}–O bond-strength is 0.16 *vu* while that of K^{+}–O is 0.10 *vu*. Acceptors of the majority of bonds from Pb^{2+} in kroupaite are apical uranyl atoms within the sheets.

URANYL-OXIDE HYDROXY-HYDRATES WITH VARIOUS INTERLAYER CATIONS

The interstitial complexes of uranyl-oxide hydrates incorporate various elements with distinct stereochemistry. Uranyl minerals form in complex multiphase chemical conditions arising from their geological settings (and geochemistry), and are also expected to form in complex environments such as underground repositories for long-term storage of nuclear (Maher et al. 2013; Ewing 2015).

Always consult and cite the final, published document. See http:/www.minsocam.org or GeoscienceWorld

The structures and compositions of uranyl-oxide hydrates have recently been reviewed (Plášil 2018a). Crystal structures of uranyl-oxide hydrates sometimes contain U(V) or U(IV), with U(V) observed in structures containing β-U_3O_8 (Burns and Finch 1999) and α-U_3O_8 (Plášil 2017a) types of uranyl-oxide layers. In nollmotzite, $Mg[U^{V}(U^{VI}O_2)_2O_4F_3]\cdot 4H_2O$, the β-$U_3O_8$ type of sheet contains fluorine as well as oxygen (Plášil et al. 2018).

The interstitial complexes of uranyl oxide hydrates incorporate various alkali and alkaline earth cations as well as lanthanides (Zhang et al. 2018, 2019; Hill and Burns 1999; Burns and Hill 2000a, b; Cahill and Burns 2000). The capacity of uranyl-oxide hydrates to accommodate cations of various Lewis-acid strengths arises in part from the heterogeneous distribution of different types of anions within the sheets: uranyl O atoms, which are somewhat undersaturated with respect to their bond-valence requirements, and OH^- groups within the uranyl-oxide layers that are bond-valence donors. These sheets readily accommodate cations of distinct charges and radii (Zhang et al. 2016), and also of different stereochemistry (Olds et al. 2017). In comparison, kamitugaite, $PbAl[(UO_2)_5(PO_4)_{2.38}(AsO_4)_{0.62}O_2(OH)_2](H_2O)_{11.5}$ (Plášil 2017b) combines divalent and trivalent cations in its interstitial complexes, and the Pb^{2+} is electron lone-pair stereoactive. The distribution of anions appears to preclude occurrence of both Pb^{2+} and Al^{3+} in the same interlayer. Thus, there are two distinct interlayers in kamitugaite, giving a large unit cell.

Voronoi-Dirichlet polyhedra (VDP) calculations (Blatov et al. 2004) were used to evaluate and quantify bonding environments in the interlayer regions of UOHs. The VDP calculations are summarized in Table 5 and selected aspects are displayed in Figure 8. Generally, Pb^{2+} occupies sites with VDP volume (V_{VDP}) ~18 Å^3. If there is an additional cation with a larger ionic radius, as K^+ in gauthierite and kroupaite, it occupies sites with V_{VDP} >20 Å^3. In leesite, the K^+ occupies a site with V_{VDP} >19.66 Å^3 that is populated by Pb^{2+} in other uranyl-oxide-hydrate

Always consult and cite the final, published document. See http:/www.minsocam.org or GeoscienceWorld

234 structures. The structure of gauthierite is particularly interesting as it contains four symmetrically
235 independent partially occupied K sites. Site K2 has V_{VDP} ~27 Å^3.

236 ## POTENTIAL Cs^+ AND Sr^{2+} INCORPORATION

237 Voronoi-Dirichlet polyhedra calculations for uranyl-oxide-hydrate structures can help in
238 predicting incorporation of radionuclides of concern for nuclear waste disposal, such as ^{135}Cs ($t^{1/2}$
239 = 2.3 MY) or ^{90}Sr ($t^{1/2}$ = 28.8 Y) that are important for long-term disposal and shorter-term heat
240 generation, respectively (Maher et al. 2013; Ewing 2015). VDP calculations are sensitive to the
241 size of the corresponding cation and can be employed to determine characteristic volumes of
242 corresponding cation polyhedra in uranyl-oxide-hydrate structures. Results of the analysis are
243 given in Table 5 and Figure 8, where bonding properties of interlayer cations in most uranyl-
244 oxide-hydrate structures based on VDP volume and corresponding ionic radii (after Shannon
245 1976) are listed. The ionic radii of Cs^+ and Sr^{2+} are 1.81 and 1.36 Å, respectively, and Sr^{2+}
246 readily substitutes for Pb^{2+} and Ca^{2+}, as in agrinierite (Cahill and Burns 2000). Substitutions of
247 Sr^{2+} for Pb^{2+} and Ca^{2+} has been documented for synthetic UOHs related to curite and becquerelite
248 (Burns and Hill 2000a; Burns and Li 2002). Cesium is less likely to be incorporated into the
249 interlayers of UOHs structures, although a synthetic uranyl oxide hydrate containing Cs has been
250 reported (Hill and Burns 1999) as well as uptake of Cs^+ by a uranyl oxide hydrate during
251 crystallization (Giammar and Hering 2004). It is plausible that Cs^+ can be incorporated in K-
252 bearing UOHs, as the V_{VDP} of K^+ sites reaches ~24 Å^3 (with an extreme value of ~27 Å^3 in case
253 of K2 in gauthierite; Tables 7).

254 ## CHARGE-DENSITY MATCH IN URANYL-OXIDE-HYDRATE STRUCTURES

Always consult and cite the final, published document. See http:/www.minsocam.org or GeoscienceWorld

We used charge density calculations to identify mis-matches in UOHs by modifying an approach used earlier for uranyl germanates and uranyl silicates (Li et al. 2018). The charge density ρ associated with the anionic structural units was calculated as $\rho = q_e \times Z/V$. Here q_e is the effective charge of the structural unit, which is the formal charge q_f of the structural units modified by the number of hydrogen bonds, $q_f + h \times 0.2$ (where h is the number of hydrogen atoms in the structural unit and 0.2 *vu* is the assumed bond-strength of the corresponding H bond). Z is the number of formula units in each unit cell, V is the unit-cell volume ($Å^3$), and ρ is then the charge density associated with the structural unit. The charge density of the interlayer complex is calculated in the same way, taking into account the formal charge of the interlayer complex modified by the H-bonds emanating from it (Table 6). The majority of UOHs structures exhibit an excess of charge density associated with the interlayer complex (Fig. 9). Exceptions are the denser (polymerized) dehydrogenated structures such as for curite and spriggite. The outlying value of the synthetic PbUOH phase (Li and Burns 2000b) is due to the density of the bond-valence acceptors within the framework as compared to the relatively simple complex occupying the channels. The high charge density of the REE^{III}-containing UOHs is associated with structural units of the α-U_3O_8 topology that are highly versatile. The variation of the charge densities for the α-U_3O_8 type sheet is the largest within the most common topological types (Table 7).

IMPLICATIONS

The new K,Pb-bearing uranyl-oxide hydroxy-hydrate kroupaite is particularly interesting due to ordering of monovalent and divalent cations of different stereochemistry in the interlayer region. Minerals provide unique insights into crystal chemical features that may be difficult to study *via* laboratory synthesis. Recent observations of natural samples, including kroupaite,

Always consult and cite the final, published document. See http:/www.minsocam.org or GeoscienceWorld

leesite and gauthierite from several localities demonstrate that uranyl-oxide-hydrate sheet anion topologies readily accommodate a range of heterovalent cations *via* unique configurations of their interlayers. Some uranyl-oxide-hydrate structures investigated here were found, based on analysis of their corresponding Voronoi-Dirichlet polyhedra, to be suitable for incorporation of large monovalent cations such as Cs^{+}.

ACKNOWLEDGEMENTS

Two anonymous reviewers as well as associate editor and structure editor are thanked for constructive comments, which improved the manuscript. This study was funded, in part, by the John Jago Trelawney Endowment to the Mineral Sciences Department of the Natural History Museum of Los Angeles County, by the Department of Energy, Basic Energy Sciences, Heavy Elements Program under grant number: DE-FG02-07ER15880, by the Czech Science Foundation (GACR 17-09161S to JP, JS and JČ), and by OP VVV project (Geobarr CZ.02.1.01/0.0/0.0/16_026/0008459 to RS).

REFERENCES

Belai, N., Frisch, M., Ilton, E.S., Ravel, B., and Cahill, C.L. (2008) Pentavalent Uranium Oxide via Reduction of $[UO_2]^{2+}$ Under Hydrothermal Reaction Conditions. Inorganic Chemistry, 47, 10135–10140.

Blatov, V.A. (2004) Voronoi–Dirichlet Polyhedra in Crystal Chemistry: Theory and Applications. Crystallography Reviews, 10, 249−318.

Brandenburg, K. (2006) DIAMOND. Crystal Impact - Dr. H. Putz & Dr. K. Brandenburg GbR, Kreuzherrenstr. 102, 53227, Bonn, Germany.

Always consult and cite the final, published document. See http:/www.minsocam.org or GeoscienceWorld

299 Brugger, J., Krivovichev, S.V., Berlepsh, P., Meisser, N., Ansermet, S., and Armbruster, T.
300 (2004) Spriggite, $Pb_3[(UO_2)_6O_8(OH)_2](H_2O)_3$, a new mineral with beta-U_3O_8-type sheets:
301 description and crystal structure. American Mineralogist, 89, 339–347.
302 Brugger, J., Meisser, N., Etschmann, B., Ansermet, S., and Pring, A. (2011) Paulscherrerite from
303 the Number 2 Workings, Mount Painter Inlier, Northern Flinders Ranges, South Australia:
304 ”Dehydrated schoepite” is a mineral after all. American Mineralogist, 96, 229–240.
305 Burns, P.C. (1997) A new uranyl-oxide-hydrate sheet in vandendriesscheite: implications for
306 mineral paragenesis and the corrosion of spent nuclear fuel. American Mineralogist, 82,
307 1176–1186.
308 Burns, P.C. (1998) The structure of compreignacite, $K_2(UO_2)_3O_2(OH)_3]_2(H_2O)_7$. Canadian
309 Mineralogist, 36, 1061–1067.
310 Burns, P.C. (1999) A new complex sheet of uranyl polyhedra in the structure of wölsendorfite.
311 American Mineralogist, 84, 1661–1673.
312 Burns, P.C. (2005) U^{6+} minerals and inorganic compounds: insights into an expanded structural
313 hierarchy of crystal structures, Canadian Mineralogist, 43, 1839–1894.
314 Burns, P.C., and Finch, R.J. (1999) Wyartite: Crystallographic evidence for the first pentavalent-
315 uranium mineral. American Mineralogist, 84, 1456–1460.
316 Burns, P.C., and Hanchar, J. (1999) The structure of masuyite, $Pb[(UO_2)_3O_8(OH)_2](H_2O)_3$, and its
317 relationship to protasite. Canadian Mineralogist, 37, 1483–1491.
318 Burns, P.C., and Hill, F.C. (2000a) Implications of the synthesis and structure of the Sr analogue
319 of curite. Canadian Mineralogist, 38, 175–181.
320 Burns, P.C., and Hill, F.C. (2000b) A new uranyl sheet in $K_5[(UO_2)_{10}O_8(OH)_9](H_2O)$: new
321 insights into sheet anion-topologies. Canadian Mineralogist, 38, 163–173.

Always consult and cite the final, published document. See http:/www.minsocam.org or GeoscienceWorld

322 Burns, P.C., and Deely, K.M. (2002) Topologically novel sheet of uranyl pentagonal bipyramids
323 in the structure of $Na[(UO_2)_4O_2(OH)_5](H_2O)_2$. Canadian Mineralogist, 40, 1579–1586.
324 Burns, P.C., and Li, Y. (2002) The structures of becquerelite and Sr-exchanged becquerelite.
325 American Mineralogist, 87, 550–557.
326 Burns, P.C., Miller, M.L., and Ewing, R.C. (1996) U^{6+} minerals and inorganic phases: a
327 comparison and hierarchy of crystal structures. Canadian Mineralogist, 34, 845–880.
328 Burns, P.C., Finch, R.J., Hawthorne, F.C., Miller, M.L., and Ewing, R.C. (1997) The crystal
329 structure of ianthinite, $[U^{4+}_2(UO_2)_4O_6(OH)_4(H_2O)_4](H_2O)_5$: a possible phase for Pu^{4+}
330 incorporation during the oxidation of spent nuclear fuel. Journal of Nuclear Materials, 249,
331 199–206.
332 Cahill, C.L., and Burns, P.C. (2000) The structure of agrinierite: a Sr-containing uranyl-oxide
333 hydrate mineral. American Mineralogist, 85, 1294–1297.
334 Casas, I., Bruno, J., Cera, E., Finch, R.J., and Ewing, R.C. (1997) Characterization and
335 dissolution behavior of a becquerelite from Shinkolobwe, Zaire. Geochimica et
336 Cosmochimica Acta, 61, 3879–3884.
337 Colmenero, F., Cobos, J., and Timón, V. (2018) Periodic Density Functional Theory Study of the
338 Structure, Raman Spectrum, and Mechanical Properties of Schoepite Mineral. Inorganic
339 Chemistry, 57, 4470–4481.
340 Colmenero, F., Plášil, J., and Němec, I. (2019) Uranosphaerite: Crystal Structure, Hydrogen
341 Bonding, Mechanics, Infrared and Raman Spectroscopy and Thermodynamics. Journal of
342 Physical Chemistry, under review.
343 Dao, N. Q. (1972) Structure cristalline de $Cs_2UO_2F_4H_2O$. Acta Crystallographica B, 28, 2011–
344 2015.

Always consult and cite the final, published document. See http:/www.minsocam.org or GeoscienceWorld

345 Ewing, R.C. (2015) Long-term storage of spent nuclear fuel. Nature Materials, 14, 252–257.

346 Finch, R.J., and Ewing, R.C. (1991) The corrosion of uraninite under oxidizing conditions.
347 Journal of Nuclear Materials, 190, 133–156.

348 Finch, R.J., Suksi, J., Rasilainen, K., and Ewing, R.C. (1996a) Uranium-series ages of secondary
349 uranium minerals with applications to the long-term evolution of spent nuclear fuel. In W.M.
350 Murphy and D.A. Knecht, Eds. Scientific Basis for Nuclear Waste Management XIX, 412,
351 823–830. Materials Research Society, Pittsburgh.

352 Finch, R.J., Cooper, M.A., Hawthorne, F.C., and Ewing, R.C. (1996b) The crystal structure of
353 schoepite, $[(UO_2)_8O_2(OH)_{12}](H_2O)_{12}$. Canadian Mineralogist, 34, 1071–1088.

354 Finch, R.J., and Murakami, T. (1999) Systematics and paragenesis of uranium minerals. In P.C.
355 Burns and R.C. Ewing, Eds., Uranium: Mineralogy, Geochemistry and the Environment.
356 Mineralogical Society of America, Chantilly, Virginia. Reviews in Mineralogy, 38, 91–179.

357 Finch, R.J., Burns, P.C., Hawthorne, F.C., and Ewing, R.C. (2006) Refinement of the crystal
358 structure of billietite $Ba[(UO_2)_6O_4(OH)_6](H_2O)_8$. Canadian Mineralogist, 44, 1197–1205.

359 Gagné, O.C., and Hawthorne, F.C (2015) Comprehensive derivation of bond-valence parameters
360 for ion pairs involving oxygen. Acta Crystallographica, B71, 562–578.

361 Ghazisaeed, S., Kiefer, B., Plášil, J. (2019) Revealing hydrogen atoms in a highly-absorbing
362 material: an X-ray diffraction study and Torque method calculations for lead-uranyl-oxide
363 mineral curite. RSC Advances, 9, 10058–10063.

364 Giammar, D.E., and Hering, J.G. (2004) Influence of dissolved sodium and cesium on uranyl-
365 oxide hydrate solubility. Environmental Science and Technology, 38, 171–179.

Always consult and cite the final, published document. See http:/www.minsocam.org or GeoscienceWorld

366 Glatz, R.E., Li, Y.P., Hughes, K.A., Cahill, C.L., and Burns, P.C. (2002) Synthesis and structure
367 of a new Ca uranyl-oxide hydrate, $Ca(UO_2)_4O_3(OH)_4)(H_2O)_2$, and its relationship to
368 becquerelite. Canadian Mineralogist, 40, 217–224.
369 Gorman-Lewis, D., Fein, J.B., Burns, P.C., Szymanowski, J.E.S., and Converse, J. (2008)
370 Solubility measurements of the uranyl-oxide hydrate phases metaschoepite, compreignacite,
371 Na–compreignacite, becquerelite, and clarkeite. Journal of Chemical Thermodynamics,40,
372 980–990.
373 Hawthorne, F.C. (2015) Toward theoretical mineralogy: A bond-topological approach. American
374 Mineralogist, 100, 696–713.
375 Hill, F.C., and Burns, P.C. (1999) The structure of synthetic Cs uranyl hydrate and its
376 relationship to compreignacite. Canadian Mineralogist, 37, 1283–1288.
377 Hloušek; J., Plášil, J., Sejkora, J., and Škácha, P. (2014) News and new minerals from Jáchymov,
378 Czech Republic (2003–2014). Bulletin mineralogicko-petrologického oddělení Národního
379 Muzea (Praha), 22, 155–181. (in Czech with English abstract).
380 Huang, J., Wang, X., and Jacobson, A.J. (2003) Hydrothermal synthesis and structures of the new
381 open-framework uranyl silicates $Rb_4(UO_2)_2(Si_8O_{20})$ (USH-2Rb), $Rb_2(UO_2)(Si_2O_6).H_2O$
382 (USH-4Rb) and $A_2(UO_2)(Si_2O_6).0.5H_2O$ (USH-5A; A = Rb, Cs). Journal of Material
383 Chemistry, 13, 191.
384 Janeczek, J., Ewing, R.C., Oversby, V.M., and Werme, L.O. (1999) Uraninite and UO_2 in spent
385 nuclear fuel: a comparison. Journal of Nuclear Materials, 238, 121–130.
386 Kirkegaard, M.C., Niedziela, J.L., Miskowiec, A., Shields, A.E., and Anderson, B.B. (2019)
387 Elucidation of the Structure and Vibrational Spectroscopy of Synthetic Metaschoepite and Its
388 Dehydration Product. Inorganic Chemistry, 58, 7310–7323.

Always consult and cite the final, published document. See http:/www.minsocam.org or GeoscienceWorld

Klingensmith, A.L., Deely, K.M., Kinman, W.S., Kelly, V., and Burns, P.C. (2007) Neptunium incorporation in sodium-substituted metaschoepite. American Mineralogist, 92, 662–669.

Krivovichev, S.V., and Burns, P.C. (2001) Crystal chemistry of uranyl molybdates. IV. The structures of $M_2((UO_2)_6(MoO_4)_7(H_2O)_2)$ (M = Cs, NH_4). Canadian Mineralogist, 39, 207–214.

Krivovichev, S.V., and Plášil, J. (2013) Mineralogy and crystallography of uranium, Uranium from cradle to grave, Vol. 43, Burns, P.C. and Sigmon, G.E. edited, MAC Short Courses, 15–119.

Kubatko, K.A., Helean, K., Navrotsky, A., and Burns, P.C. (2006a) Thermodynamics of uranyl minerals: Enthalpies of formation of uranyl oxide hydrates. American Mineralogist, 91, 658–666.

Kubatko, K.-A., and Burns, P.C. (2006b) Cation−Cation Interactions in $Sr_5(UO_2)_{20}(UO_6)_2O_{16}(OH)_6(H_2O)_6$ and $Cs(UO_2)_9U_3O_{16}(OH)_5$. Inorganic Chemistry, 45, 10277–10281.

Li, Y., and Burns, P.C. (2000a) Investigations of crystal-chemical variability in lead uranyl-oxide hydrates. II. Fourmarierite. Canadian Mineralogist, 38, 737–749.

Li, Y., and Burns, P.C. (2000) Synthesis and crystal structure of a new Pb uranyl-oxide hydrate with a framework structure that contains channels. Canadian Mineralogist, 38, 1433–1441.

Li, Y., and Burns, P.C. (2000) The structures of two sodium uranyl compounds relevant to nuclear waste disposal. Journal of Nuclear Materials, 299, 219–226.

Li, Y., Cahill, C.L., and Burns, P.C. (2001) Synthesis, Structural Characterization, and Topological Rearrangement of a Novel Open Framework U−O Material: $(NH_4)_3(H_2O)_2\{[(UO_2)_{10}O_{10}(OH)][(UO_4)(H_2O)_2]\}$. Chemistry of Materials, 13, 4026–4031.

Always consult and cite the final, published document. See http:/www.minsocam.org or GeoscienceWorld

Li, H., Langer, E.M., Kegler, P., Modolo, G., and Alekseev, E.V. (2018) Formation of Open Framework Uranium Germanates: The Influence of Mixed Molten Flux and Charge Density Dependence in U-Silicate and U-Germanate Families. Inorganic Chemistry, 57, 11201−11216.

Libowitzky, E. (1999) Correlation of O–H stretching frequencies and O–H···O hydrogen bond lengths in minerals. Monatshefte für Chemie, 130, 1047–1059.

Locock, A.J., and Burns, P.C. (2003) Structures and synthesis of framework Rb and Cs uranyl arsenates and their relationships with their phosphate analogues. Journal of Solid State Chemistry, 175, 372–379.

Lussier, A.J., Lopez, R.A.K., and Burns, P.C. (2016) A revised and expanded structure hierarchy of natural and synthetic hexavalent uranium compounds. Canadian Mineralogist, 54, 177–283.

Maher, K., Bargar, J.R., and Brown, G. E., Jr. (2013) Environmental speciation of actinides. Inorganic Chemistry, 52, 3510–3532.

Mandarino, J.A. (2007) The Gladstone–Dale compatibility of minerals and its use in selecting mineral species for further study. Canadian Mineralogist, 45, 1307-1324.

Obbade, S., Dion, C., Saadi, M., and Abraham, F. (2004) Synthesis, crystal structure and electrical characterization of $Cs_4((UO_2)_2(V_2O_7)O_2)$, a uranyl divanadate with chains of corner-sharing uranyl square bipyramids. Journal of Solid State Chemistry, 177, 1567–1574.

Olds, T.A., Plášil, J., Kampf, A.R., Škoda, R., Burns, P.C., Čejka, J., Bourgoin, V., and Boulliard, J.-C. (2017) Gauthierite, $KPb[(UO_2)_7O_5(OH)_7]\cdot 8H_2O$, a new uranyl-oxide hydroxy-hydrate mineral from Shinkolobwe with a novel uranyl-anion sheet-topology. European Journal of Mineralogy, 29, 129–141.

Always consult and cite the final, published document. See http:/www.minsocam.org or GeoscienceWorld

435 Olds, T., Plášil, J., Kampf, A.R., Spano, T., Haynes, P., Carlson, S.M., Burns, P.C., Simonetti,
436 A., and Mills, O.P. (2018) Leesite, $K(H_2O)_2[(UO_2)_4O_2(OH)_5]\cdot 3H_2O$, a new K-bearing
437 schoepite-family mineral from the Jomac mine, San Juan County, Utah, U.S.A. American
438 Mineralogist, 103, 143–150.
439 Ondruš, P., Veselovský, F., Gabašová, A., Hloušek, J., Šrein, V., Vavřín, I., Skála, R., Sejkora, J.,
440 and Drábek, M. (2003) Primary minerals of the Jáchymov ore district. Journal of the Czech
441 Geological Society, 48, 19–147.
442 Pagoaga, M.K., Appleman, D.E., and Stewart, J.M. (1987) Crystal structures and crystal
443 chemistry of the uranyl-oxide hydrates becquerelite, billietite, and protasite. American
444 Mineralogist, 72, 1230–1238.
445 Petříček, V., Dušek, M., and Palatinus, L. (2014) Crystallographic Computing System Jana 2006:
446 general features. Zeitschrift für Kristallographie, 229, 345–352.
447 Plášil, J. (2014) Oxidation-hydration weathering of uraninite: the current state-of-knowledge,
448 Journal of Geosciences, 59, 89–114.
449 Plášil, J. (2017a) Crystal structure of richetite revisited: Crystallographic evidence for the
450 presence of pentavalent uranium. American Mineralogist, 102, 1171–1175.
451 Plášil, J. (2017b) A novel sheet topology in the structure of kamitugaite,
452 $PbAl[(UO_2)_5(PO_4)_{2.38}(AsO_4)_{0.62}O_2(OH)_2](H_2O)_{11.5}$. Journal of Geosciences, 62, 253–260.
453 Plášil, J. (2018a) Uranyl-oxide hydroxy-hydrate minerals: their structural complexity and
454 evolution trends. European Journal of Mineralogy, 30, 237–251.
455 Plášil, J. (2018b) The crystal structure of uranyl-oxide mineral schoepite, $[(UO_2)_4O(OH)_6](H_2O)_6$,
456 revisited. Journal of Geosciences, 63, 65–73.

Always consult and cite the final, published document. See http:/www.minsocam.org or GeoscienceWorld

Plášil, J. (2019) Hydrogen bonding in lead uranyl-oxide mineral sayrite. Zeitschrift für Kristallographie, DOI: 10.1515/zkri-2019-0035.

Plášil, J., Škoda, R., Čejka, J., Bourgoin, V., and Boulliard, J.-C. (2016) Crystal structure of the uranyl-oxide mineral rameauite. European Journal of Mineralogy, 28, 959–967.

Plášil, J., Kampf, A.R., Škoda, R., and Čejka, J. (2018) Nollmotzite, $Mg[U^{V}(U^{VI}O_2)_2O_4F_3]\cdot 4H_2O$, the first natural uranium oxide containing fluorine. Acta Crystallographica B, 74, 362–369.

Pouchou, J.-L., and Pichoir, F. (1991) Quantitative analysis of homogeneous or stratified microvolumes applying the model "PAP." In K.F.J. Heinrich and D.E. Newbury, Eds., Electron Probe Quantitation, pp. 3l–75. Plenum Press.

Rigaku (2019). CrysAlis CCD and CrysAlis RED. Oxford Diffraction Ltd, Yarnton, Oxfordshire, UK.

Shannon, R.D. (1976) Revised effective ionic radii and systematic studies of interatomic distances in halides and chalcogenides. Acta Crystallographica A, 32, 751–767.

Sheldrick, G.M. (2015) Crystal structure refinement with SHELXL. Acta Crystallographica, C71, 3–8.

Walenta, K., and Theye, T. (2012) Heisenbergite, a new uranium mineral from the uranium deposit of Menzenschwand in the Southern Black Forest, Germany. Neues. Jahrbuch für Mineralogie Abhandlungen, 189/2, 117–123.

Walker, T.L. (1923) Schoepite, a new mineral from Kasolo, Belgian Congo. American Mineralogist, 8, 67−69.

Weller, M.T., Light, M.E., and Gelbrich, T. (2000) Structure of uranium(VI) oxide dihydrate, $UO_3\cdot 2H_2O$; synthetic meta-schoepite $[(UO_2)_4O(OH)_6]\cdot_5H2O$. Acta Crystallographica B, 6, 577–583.

Always consult and cite the final, published document. See http:/www.minsocam.org or GeoscienceWorld

Wylie, E.M., and Burns, P.C. (2012) Crystal structures of six new uranyl selenate and selenite compounds and their relationship with uranyl mineral structures. Canadian Mineralogist, 50, 147–157.

Wronkiewicz, D.J., Bates, J.K., Wolf, S.F., and Buck, E.C. (1996) Ten-year results from unsaturated drip tests with UO_2 at 90°C: implications for the corrosion of spent nuclear fuel. Journal of Nuclear Materials, 238, 78–95.

Zhang, Y., Čejka, J., Lumpkin, G.R., Tran, T.T., Aharonovich, I., Karatchevtseva, I., Price, J.R., Scales, N., and Lu, K. (2016) Hydrothermal synthesis, structures and properties of two uranyl oxide-hydroxyl hydrate pahses with Co(II) or Ni(II) ions. New Journal of Chemistry, 40, 5357–5363.

Zhang, Y., Aughterson, R., Karatchevtseva, I., Kong, L., Trong Tran, T., Čejka, J., Aharonovich, I., and Lumpkin, G.R. (2018) Uranyl-oxide hydrate phases with heavy lanthanide ions: $[Ln(UO_2)_2O_3(OH)]\cdot 0.5H_2O$ (Ln = Tb, Dy, Ho and Yb). New Journal of Chemistry, 42, 12267–13184.

Zhang, Y., Aughterson, R., Zhang, Z., Wei, T., Lu, K., Čejka, J., and Karatchevtseva, I. (2019) Syntheses, Crystal Structures and Spectroscopic Studies of Uranyl-Oxide Hydrate Phases with La(III)/Nd(III) Ions. Inorganic Chemistry, 58, 10812–10821.

Always consult and cite the final, published document. See http:/www.minsocam.org or GeoscienceWorld

497

498 FIGURE CAPTIONS

499 Figure 1. Orange yellow aggregates of kroupaite on the surface of strongly altered uraninite.
500 Horizontal field of view is 2.5 mm (photo P. Škácha).

501

502 Figure 2. Crystal drawing of kroupaite in clinographic projection.

503

504 Figure 3a. Raman spectrum of kroupaite in the full-range (4500–12 cm^{-1}, split at 2000 cm^{-1}).

505 Figure 3b). Band decomposition in the Raman spectrum of kroupaite for ν_1 $(UO_2)^{2+}$ in the region
506 from 950–700 cm^{-1}.

507

508 Figure 4. Crystal structure of kroupaite viewed down [001]. The uranyl-oxide hydroxide sheets
509 (in yellow) alternate with the interlayer containing water oxygen (red), potassium (lavender) and
510 lead (orange). Unit-cell edges are outlined by black-solid lines.

511

512 Figure 5. Comparative view of the anion sheet topologies and OH^- distributions for uranyl-oxide
513 hydroxide-hydrate minerals with the fourmarierite topology. Black circles highlight vertices
514 containing OH^-, and bare vertices represent O^{2-}; orange spheres represent Pb^{2+}, blue K^+, and
515 green Na^+ atoms, respectively. Figure adapted from Klingensmith et al. (2007).

516

Always consult and cite the final, published document. See http:/www.minsocam.org or GeoscienceWorld

Figure 6. Ternary compositional plot for chemical analyses of kroupaite and related minerals. Analyses from additional set of kroupaite samples (labelled as JACH) are displayed to illustrate chemical substitutional trends. $M^{+} \leftrightarrow$ vacancy (with black dashed line): variability in composition between leesite (end-member) and schoepite; $M^{+} \leftrightarrow M^{2+}$ (black solid line): variability between leesite (end-member) and fourmarierite; the grey arrow points towards the substitution characteristic for intermediate series members and schoepite.

Figure 7. Voronoi-Dirichlet polyhedra (VDP) for interlayer cations in selected structures with corresponding VDP volumes (V_{VDP}): a) kroupaite, K1 atom (lavender); Pb1 atom (orange); b) leesite; K1 atom (lavender); c) fourmarierite.

Figure 8. The size of cation polyhedra in the interlayers of uranyl-oxide hydroxy-hydrate structures: the volume (V_{VDP}) of Voronoi-Dirichlet polyhedra versus the ionic radius. Outliers are labelled.

Figure 9. Charge-density matches in uranyl-oxide hydrate structures. The black solid line represents a linear fit to the data (equation and regression statistics given), and the dashed line represent an ideal match; $a = -1$, $b = 0$.

Always consult and cite the final, published document. See http:/www.minsocam.org or GeoscienceWorld

This is a preprint, the final version is subject to change, of the American Mineralogist (MSA)
Cite as Authors (Year) Title. American Mineralogist, in press.
DOI: https://doi.org/10.2138/am-2020-7311

Table 1. Analytical data for kroupaite (in wt. %), average of 6 analyses.

Constituent	Mean	Range	Stand. Dev.	Probe Standard	Normalised
Na_2O	0.08	0.00–0.20	0.08	albite	0.08
K_2O	2.14	1.99–2.32	0.10	sanidine	2.25
CaO	0.10	0.08–0.14	0.03	fluorapatite	0.10
PbO	1.84	1.64–2.46	0.31	vanadinite	1.93
CuO	0.41	0.00–0.72	0.28	lammerite	0.43
CoO	0.05	0.00–0.33	0.12	Co metal	0.05
Al_2O_3	0.02	0.00–0.12	0.04	sanidine	0.02
Bi_2O_3	0.25	0.00–0.51	0.19	Bi metal	0.26
UO_3	80.67	78.80–82.24	1.15	uranophane	84.64
SO_3	0.11	0.00–0.38	0.18	$SrSO_4$	0.12
H_2O*	9.65				10.12
Total	95.23				100.00

*calculated as determined from the structure.

Always consult and cite the final, published document. See http:/www.minsocam.org or GeoscienceWorld

This is a preprint, the final version is subject to change, of the American Mineralogist (MSA)
Cite as Authors (Year) Title. American Mineralogist, in press.
DOI: https://doi.org/10.2138/am-2020-7311

Table 2. Powder X-ray data (*d* in Å) for kroupaite.

I_{obs}	d_{obs}	d_{calc}	I_{calc}	*hkl*	I_{obs}	d_{obs}	d_{calc}	I_{calc}	*hkl*
100	**7.407**	7.4101	100	2 0 0			2.0493	8	0 6 4
		6.4972	2	0 2 1	**21**	**2.0348**	2.0372	11	6 2 4
		4.4916	3	3 1 1			2.0226	5	6 4 0
		3.7050	21	4 0 0			2.0166	5	2 0 8
59	**3.602**	3.6025	35	0 2 4	**11**	**1.9777**	1.9752	10	2 6 4
		3.5240	16	0 4 0	4	1.8526	1.8525	3	8 0 0
78	**3.224**	3.2399	53	2 2 4			1.8241	4	4 0 8
		3.1824	23	2 4 0	**10**	**1.7984**	1.8012	4	0 4 8
		2.8581	2	5 1 1			1.7933	7	4 6 4
		2.7655	3	2 4 3	7	1.7474	1.7503	5	2 4 8
16	**2.572**	2.5828	15	4 2 4			1.7142	3	2 8 0
		2.5534	7	4 4 0			1.6475	5	8 2 4
		2.4700	4	6 0 0	7	1.6471	1.6397	2	8 4 0
		2.3266	2	0 6 1			1.6388	3	2 8 3
		2.1660	2	1 4 6			1.6358	2	2 6 7
6	2.0886	2.0957	4	0 0 8	6	1.6238	1.6199	4	4 4 8
		2.0775	2	7 1 1			1.5980	2	6 0 8
					5	1.5864	1.5929	2	2 2 10
							1.5772	3	6 6 4

Always consult and cite the final, published document. See http:/www.minsocam.org or GeoscienceWorld

Table 3. Selected interatomic distances (Å) for kroupaite.

U1–O2	1.805(10)	U2–O11	1.789(11)	U3–O4	1.765(10)
U1–O7	1.799(11)	U2–O14	1.799(12)	U3–O8	1.800(10)
U1–O1^{i}	2.231(9)	U2–O1	2.222(8)	U3–O6	2.413(9)
U1–O6	2.693(10)	U2–O10^{iii}	2.548(9)	U3–O9	2.451(9)
U1–O10^{ii}	2.460(8)	U2–O12^{iii}	2.428(10)	U3–O11	2.533(9)
U1–O13	2.254(8)	U2–O18^{ii}	2.312(9)	U3–O12	2.224(9)
U1–O22	2.434(9)	U2–O22	2.445(9)	U3–O16	2.313(9)
$<U1–O_{Ur}>$	1.80	$<U2–O_{Ur}>$	1.79	$<U3–O_{Ur}>$	1.78
$<U1–O_{eq}>$	2.41	$<U2–O_{eq}>$	2.39	$<U3–O_{eq}>$	2.39
U4–O3	1.791(12)	Pb1–O4^{iii}	2.971(11)	K1–O4^{vii}	3.201(18)
U4–O5	1.797(10)	Pb1–O5^{v}	2.804(11)	K1–O6^{vii}	2.902(18)
U4–O1	2.252(8)	Pb1–O7^{v}	3.025(11)	K1–O8^{xi}	3.201(18)
U4–O6^{iv}	2.410(9)	Pb1–O7^{iv}	3.102(11)	K1–O15	2.86(2)
U4–O11	2.471(10)	Pb1–O8^{v}	2.803(11)	K1–O16^{xi}	3.28(2)
U4–O12	2.253(9)	Pb1–O10	2.732(11)	K1–O17	2.86(2)
U4–O19	2.538(9)	Pb1–O14	2.462(14)	K1–O18	2.69(3)
$<U4–O_{Ur}>$	1.79	Pb1–O14^{vi}	3.036(14)	$<K1–O>$	3.00
$<U4–O_{eq}>$	2.39	Pb1–O18^{vii}	3.006(16)		
		$<Pb1–O>$	2.88		

Symmetry codes: (i) $–x+3/2, y–1/2, z$; (ii) $–x+3/2, –y+1, z–1/2$; (iii) $x, –y+3/2, z–1/2$; (iv) $–x+3/2, y+1/2, z$; (v) $x–1/2, –y+3/2, –z+1$; (vi) $–x+1, –y+2, –z+1$; (vii) $–x+1, –y+1, –z+1$; (viii) $–x+1, y+1/2, –z+3/2$; (ix) $x, –y+3/2, z+1/2$; (x) $x+1/2, –y+3/2, –z+1$; (xi) $x+1/2, y, –z+3/2$; (xii) $–x+3/2, –y+1, z+1/2$.

Always consult and cite the final, published document. See http:/www.minsocam.org or GeoscienceWorld

This is a preprint, the final version is subject to change, of the American Mineralogist (MSA)
Cite as Authors (Year) Title. American Mineralogist, in press.
DOI: https://doi.org/10.2138/am-2020-7311

Table 4. The bond-valence analysis for krouapite.*

	U1	U2	U3	U4	Pb1#	K1#	ΣBV_{anions}	Assignment
O1	0.68	0.69		0.65			2.01	O
O2	1.66						1.66	O
O3				1.71			1.71	O
O4			1.81		0.12	0.06	1.99	O
O5				1.69	0.17		1.87	O
O6	0.25		0.46	0.46		0.12	1.29	OH
O7	1.69				0.19		1.88	O
O8			1.68		0.17	0.06	1.91	O
O9	0.42	0.35	0.42				1.19	OH
O10		1.72			0.21		1.93	O
O11		0.45	0.36	0.41			1.21	OH
O12	0.64		0.69	0.65			1.98	O
O13		1.69					1.69	O
O14					0.48		0.48	H_2O
O15						0.13	0.13	H_2O
O16		0.57	0.57			0.05	1.18	OH
O17						0.13	0.13	H_2O
O18					0.11	0.20	0.31	H_2O
O19	0.44	0.43		0.35			1.22	OH
$\Sigma BV_{cations}$	5.78	5.89	5.99	5.92	1.46	0.73		

*All values are in valence units (*vu*); # – site with a reduced occupancy; ∑BV – sum of the bond-valences; bond–valence parameters were taken from Gagné & Hawthorne (2015) and from Burns et al. (1997).

Always consult and cite the final, published document. See http:/www.minsocam.org or GeoscienceWorld

Table 5. Crystal-chemical characteristics for metal cations and their coordination environment in structures of selected minerals and compounds.

Structure	Atom	CN	Ionic radius (Å)	V_{VDP} (Å^3)
Kroupaite (this work)	K	9	1.55	23.331
	Pb	9	1.35	19.0646
Leesite (Olds et al. 2018)	K	9	1.55	19.6591
Fourmarierite (Li and Burns 2000a)	Pb1	7	1.23	16.2588
	Pb2	9	1.35	18.3776
Gauthierite (Olds et al. 2017)	Pb1	9	1.35	15.432
	Pb2	10	1.4	19.095
	Pb3	10	1.4	22.429
	Pb4	11	1.45	18.342
	K1	12	1.64	22.905
	K2	10	1.59	27.398
	K3	10	1.59	22.451
Na-metaschoepite (Klingensmith et al. 2007)	Na	5	1	9.987
CsUOH (Hill and Burns 1999)	Cs	10	1.81	29.668
CsUSi (Huang et al. 2003)	Cs	10	1.81	27.183
	Cs	9	1.78	28.804
	Cs	10	1.81	25.721
	Cs		1.88	30.621
Wölsendorite (Burns 1999)	Pb1	8	1.29	17.758
	Pb2	11	1.45	17.354
	Pb3	11	1.45	16.974
	Pb4	9	1.35	16.971
	Pb5	11	1.45	17.055
	Pb6	11	1.45	18.604
	Pb7	7	1.23	14.645
	Pb8	10	1.4	22.77
Vandendriesscheite (Burns 1997)	Pb1	9	1.35	15.863
	Pb2	10	1.4	18.035
Sr-curite (Burns and Hill 2000a)	Sr1	10	1.36	16.146
	Sr2	11	1.4	15.927
Sr-becquerelite (Burns and Li 2002)	Sr1	11	1.4	17.338
	Sr2	11	1.4	14.875
Agrinierite (Cahill and Burns 2000)	Ca/Sr	9	1.31	13.501
Spriggite (Brugger et al. 2004)	Pb1	11	1.45	14.439
	Pb2	8	1.29	16.073
	Pb3	10	1.4	16.973
	Pb4	10	1.4	17.377
	Pb5	9	1.35	16.805
	Pb6	9	1.35	16.909
	Pb7	8	1.29	13.25

Always consult and cite the final, published document. See http:/www.minsocam.org or GeoscienceWorld

Rameauite (Plášil et al. 2016)	K1	12	1.64	20.283
	K2	12	1.64	19.433
	Ca	10	1.23	13.658
Richetite (Plášil 2017a)	Pb1	10	1.4	18.172
	Pb2	10	1.4	16.689
	Pb3	11	1.45	16.76
	Pb4	11	1.45	16.811
	Pb5	10	1.4	15.754
	Fe/Mg	6	0.74	8.867
	Pb6	10	1.4	16.253
	Pb7	9	1.35	16.763
	Pb8	11	1.45	16.9
KUOH (Burns and Hill 2000b)	K1	8	1.51	21.516
	K2	11	1.61	21.165
	K3	9	1.55	19.698
	K4	10	1.59	22.164
	K5	10	1.59	18.619
	K6	11	1.61	19.045
	K7	11	1.61	20.121
	K8	12	1.64	19.871
	K9	11	1.61	20.287
	K10	10	1.59	21.009
Becquerelite (Burns and Li 2002)	Ca	8	1.12	13.066
Billietite (Finch et al. 2006)	Ba	10	1.52	18.199
Compreignacite (Burns 1998)	K	7	1.46	11.198
Curite (Ghazisaeed et al. 2019)	Pb1	9	1.35	13.015
	Pb2	10	1.4	16.142
Masuyite (Burns and Hanchar 1999)	Pb1	10	1.4	16.135
	Pb2	12	1.49	16.577
Protasite (Pagoaga et al. 1987)	Ba	10	1.52	17.171
Sayrite (Plášil 2019)	Pb	9	1.35	16.682
Wyartite (Burns and Finch 1999)	Ca	7	1.06	17.746
Nollmotzite (Plášil et al. 2018)	Mg	6	0.72	8.657
PbUOH (Li and Burns 2000b)	Pb	8	1.29	14.733
K_2CoUOH (Zhang et al. 2016)	Co	6	0.75	8.772
	K1	12	1.64	19.417
	K2	10	1.59	19.729
K_2NiUOH (Zhang et al. 2016)	Ni	6	0.69	8.464
	K1	12	1.64	19.484
	K2	10	1.59	19.719
CsUOH (Kubatko et al. 2006b)	Cs	12	1.88	24.082
CsUV (Obbade et al. 2004)	Cs2	12	1.88	26.135
	Cs1	12	1.88	27.807
	Cs3	12	1.88	27.284

Always consult and cite the final, published document. See http:/www.minsocam.org or GeoscienceWorld

CsUMo (Krivovichev and Burns 2001)	Cs2	12	1.88	28.63
	Cs1	12	1.88	24.171
CsCoUSe (Wylie and Burns 2012)	Cs	9	1.78	15.689
CsAsU (Locock and Burns 2003)	Cs2	12	1.88	32.097
	Cs1	12	1.88	31.874
CsUFO (Dao 1972)	Cs1	11	1.85	26.894
	Cs2	10	1.81	26.166

CN – coordination number; V_{VDP} – volume of the corresponding Voronoi-Dirichlet polyhedron.

Always consult and cite the final, published document. See http:/www.minsocam.org or GeoscienceWorld

Table 6. Charge-densities of structural units and interlayer complexes in selected UOHs.

Structure	q	$q_{effective}$	Z	V	ρ^-	ρ^+
Schoepite (Plášil 2018b)	0	-1.2	8	3528.22	0	-0.00272
Metaschoepite (Weller et al. 2000)	0	-1.2	8	3429.97	0	-0.0028
Kroupaite (this work)	-2	-4	4	3502.3	-0.00228	-0.00457
Leesite (Olds et al. 2018)	-1	-2	8	3522	-0.00227	-0.00454
Fourmarierite (Li and Burns 2000a)	-2	-2.8	8	3280	-0.00488	-0.00683
Na-metaschoepite (Klingensmith et al. 2007)	-1	-2	8	3452.96	-0.00232	-0.00463
Gauthierite (Olds et al. 2017)	-3	-4.4	8	5917.8	-0.00406	-0.00595
Vandendriesscheite (Burns 1997)	-3	-5.2	8	8490	-0.00283	-0.0049
Curite (Ghazisaeed et al. 2019)	-6	-7.2	2	1367.78	-0.00877	-0.01053
Sr-curite (Burns and Hill 2000a)	-5.64	-6.912	2	1341.5	-0.00841	-0.0103
CsUOH (Hill and Burns 1999)	-3	-5.6	3	3871.16	-0.00232	-0.00434
KUOH (Burns and Hill 2000b)	-5	-6.8	4	3549.5	-0.00563	-0.00766
Compreignacite (Burns 1998)	-2	-3.2	2	1299.3	-0.00308	-0.00493
Wölsendorfite (Burns 1999)	-14	-14.8	8	10982	-0.0102	-0.01078
Masuyite (Burns and Hanchar 1999)	-2	-2.4	2	599	-0.00668	-0.00801
Agrinierite (Cahill and Burns 2000)	-4	-4.8	8	4799.6	-0.00667	-0.008
PbUOH (Li and Burns 2000b)	-5	-7	4	3450	-0.0058	-0.00812
NaUOH (Li and Burns 2001)	-2	-2.4	4	967.33	-0.00827	-0.00992
NH_4UOH (Li et al. 2001)	-3	-4	4	3512	-0.00342	-0.00456
NaUOH (Burns and Deely 2002)	-1	-2	2	715.97	-0.00279	-0.00559
Sr-becquerelite (Burns and Li 2002)	-2.54	-2.832	1	298.4	-0.00851	-0.00949
Becquerelite (Burns and Li 2002)	-2	-3.2	4	2563.1	-0.00312	-0.00499
CaUOH (Glatz et al. 2002)	-2	-2.8	2	649.6	-0.00616	-0.00862
Uranosphaerite (Colmenero et al. 2019)	0	-0.2	4	453.6	0	-0.00176
Billietite (Finch et al. 2006)	-2	-3.2	4	2614.7	-0.00306	-0.0049
Rameauite (Plášil et al. 2016)	-4	-4.8	4	2437.7	-0.00656	-0.00788
Nollmotzite (Plášil et al. 2018)	-2	-2.6	2	676.98	-0.00591	-0.00768
Sayrite (Plášil 2019)	-4	-4.4	2	964.46	-0.00829	-0.00912
Spriggite (Brugger et al. 2004)	-6	-6.4	8	4616	-0.0104	-0.01109
Richetite (Plášil 2017a)	-11	-13.8	2	3600.68	-0.00611	-0.00767
Protasite (Pagoaga et al. 1987)	-2	-2.4	2	617.497	-0.00648	-0.00777
Vandenbrandeite (Rosenzweig and Ryan 1977)	0	-0.8	2	254.929	0	-0.00628
K_2CoUOH (Zhang et al. 2016)	-3	-5.6	1	2509.2	-0.0012	-0.00223
K_2NiUOH (Zhang et al. 2016)	-3	-5.6	1	2500.3	-0.0012	-0.00224
La_3UOH (Zhang et al. 2019)	-9	-10	2	1124	-0.01601	-0.01779
Nd_3UOH (Zhang et al. 2019)	-9	-10	2	1097	-0.01641	-0.01823
U^VUOH (Belai et al. 2008)	0	-1	4	1254	0	-0.00319
Ianthinite (Burns et al. 1997)	0	-2.4	4	2502.7	0	-0.00384

Always consult and cite the final, published document. See http:/www.minsocam.org or GeoscienceWorld

q – charge; $q_{effective}$ – effective charge (charge modified by the number and strength of H bonds); Z – formula units; V – unit-cell volume (Å^3); ρ^- – charge-density of structural units (e Å^{-3}); ρ^+ – charge-density of interlayer complex (e Å^{-3}).

Table 7. Ranges in charge-densities for most common topological types of UOH structural units.

Topology	Charge density range (eÅ^{-3})	Range in Lewis basicity (*vu*)
α-U_3O_8	2.23×10^{-3}–18.23×10^{-3}	0.14–0.23
β-U_3O_8	3.84×10^{-3}–11.09×10^{-3}	0.12–0.24
fourmarierite	2.72×10^{-3}–6.83×10^{-3}	0.11–0.23

Always consult and cite the final, published document. See http:/www.minsocam.org or GeoscienceWorld

This is a preprint, the final version is subject to change, of the American Mineralogist (MSA)
Cite as Authors (Year) Title. American Mineralogist, in press.
DOI: https://doi.org/10.2138/am-2020-7311

Fig. 1

Always consult and cite the final, published document. See http:/www.minsocam.org or GeoscienceWorld

This is a preprint, the final version is subject to change, of the American Mineralogist (MSA)
Cite as Authors (Year) Title. American Mineralogist, in press.
DOI: https://doi.org/10.2138/am-2020-7311

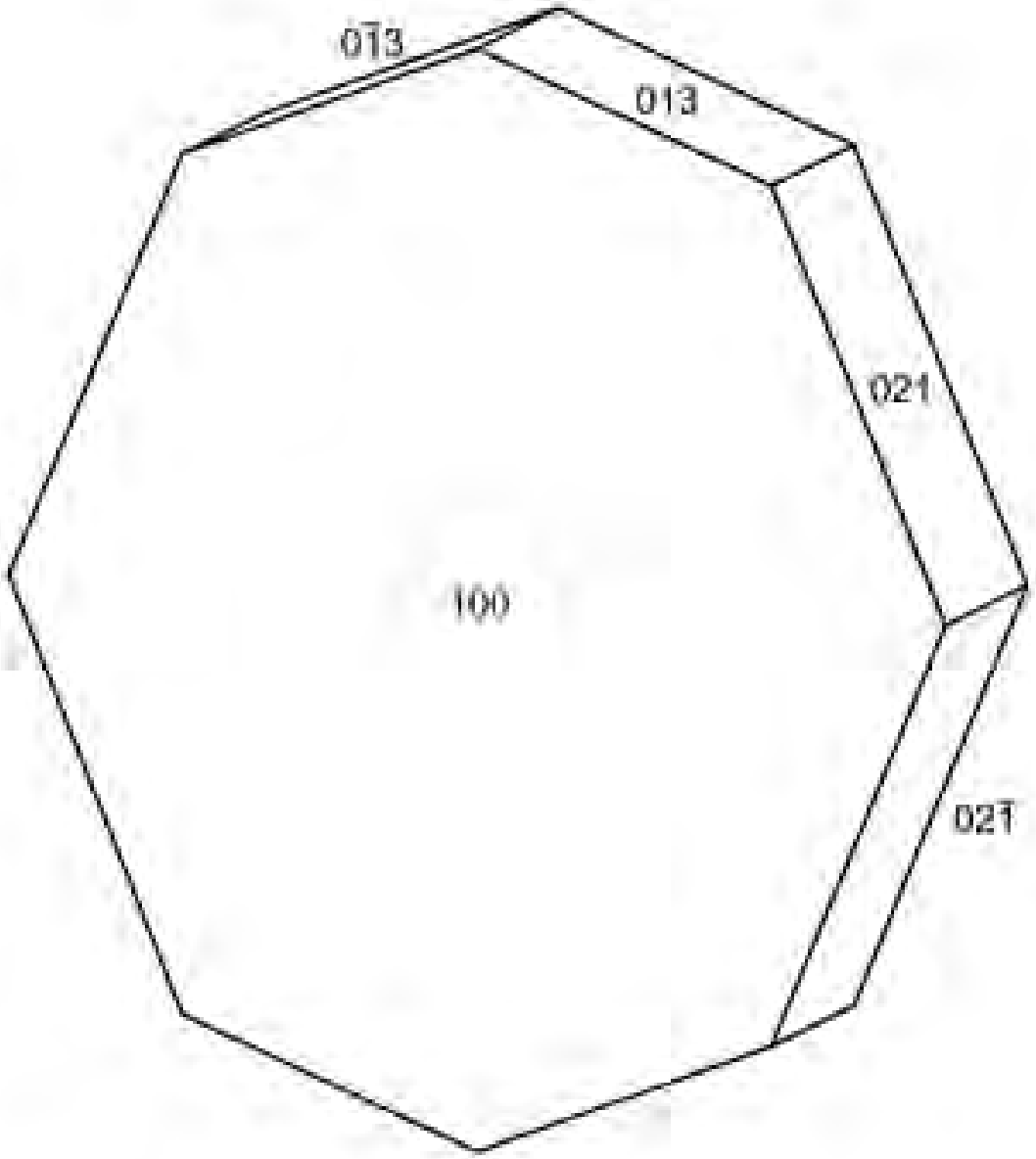

Fig. 2

Always consult and cite the final, published document. See http:/www.minsocam.org or GeoscienceWorld

This is a preprint, the final version is subject to change, of the American Mineralogist (MSA)
Cite as Authors (Year) Title. American Mineralogist, in press.
DOI: https://doi.org/10.2138/am-2020-7311

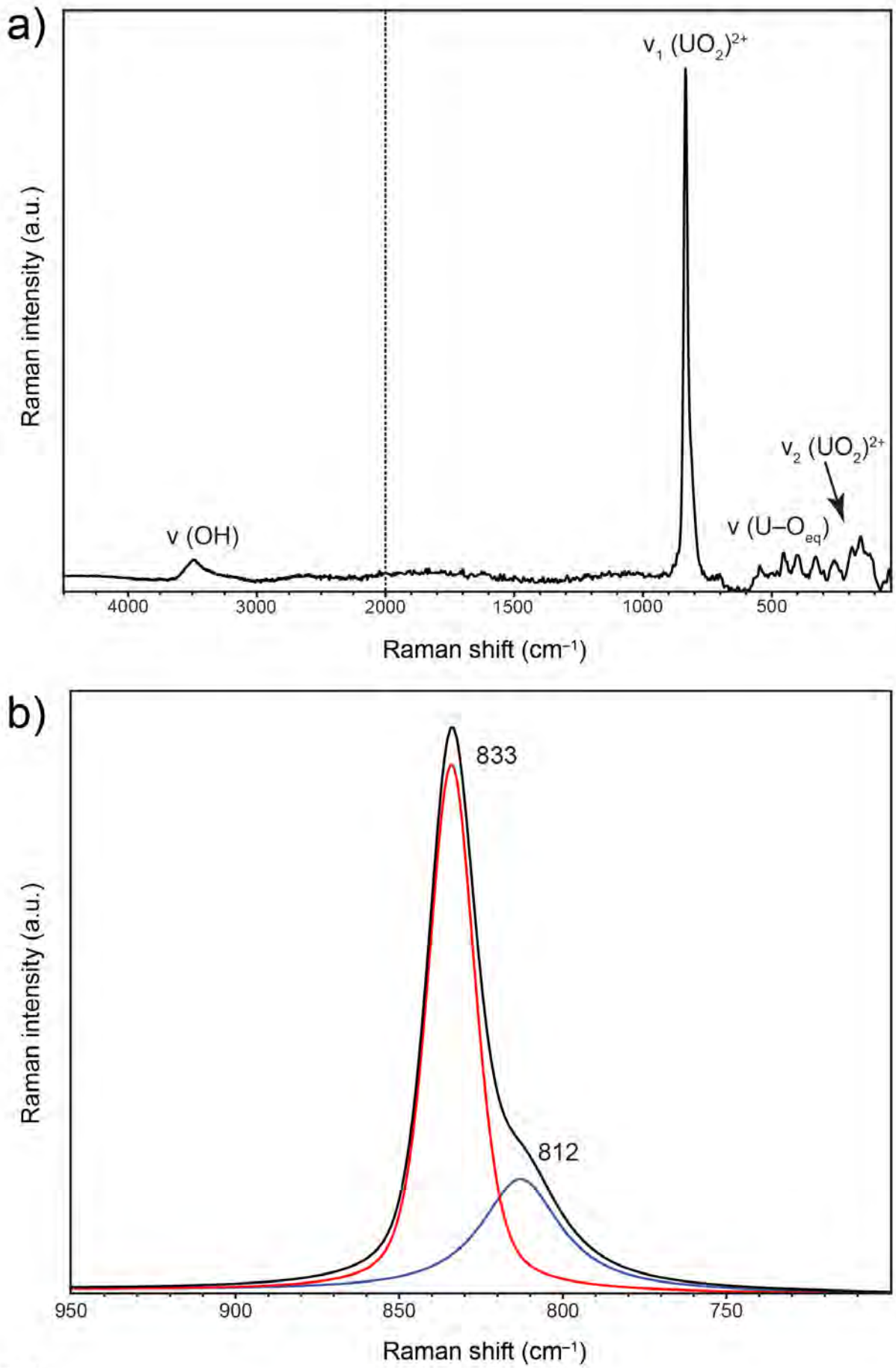

Fig. 3

Always consult and cite the final, published document. See http:/www.minsocam.org or GeoscienceWorld

This is a preprint, the final version is subject to change, of the American Mineralogist (MSA)
Cite as Authors (Year) Title. American Mineralogist, in press.
DOI: https://doi.org/10.2138/am-2020-7311

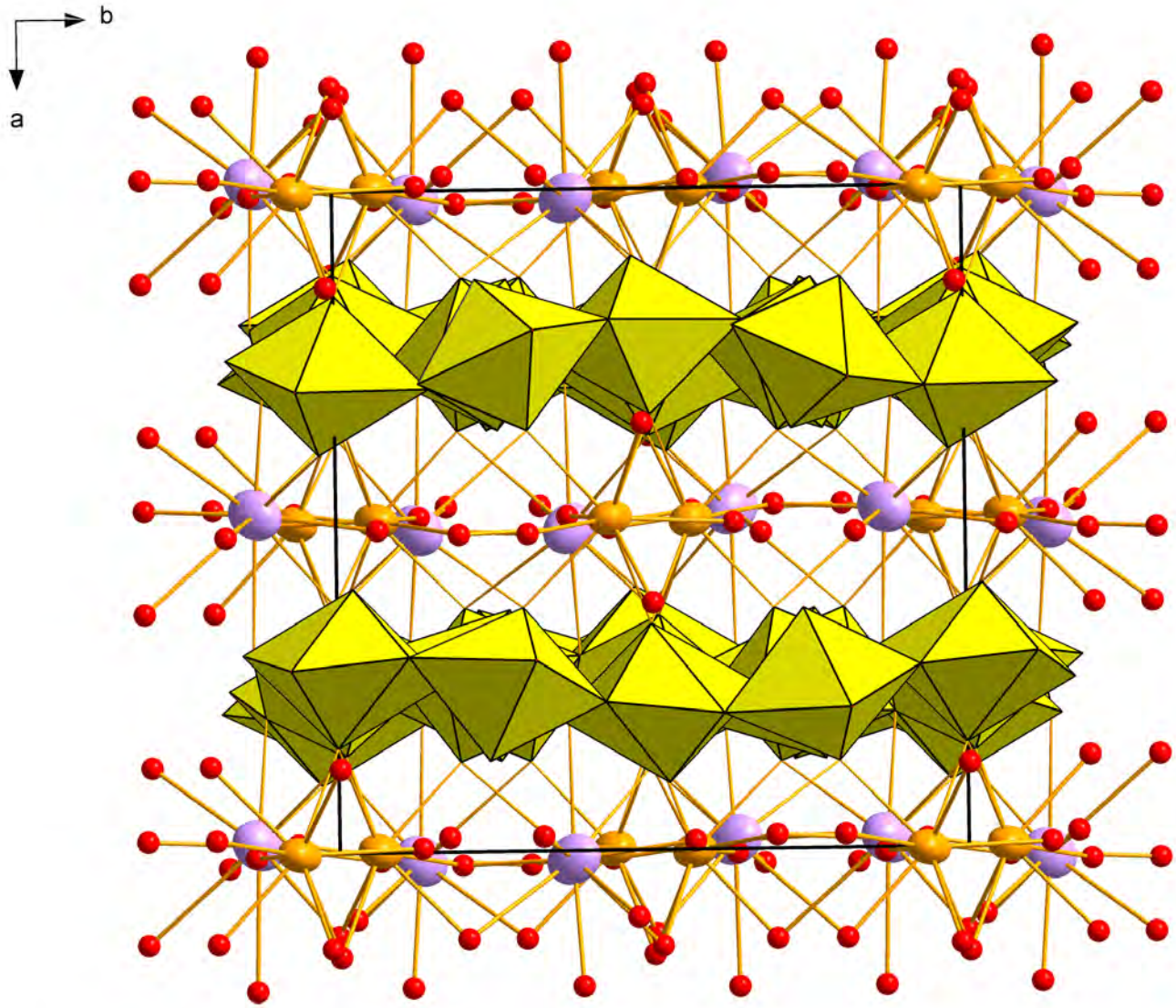

Fig. 4

Always consult and cite the final, published document. See http:/www.minsocam.org or GeoscienceWorld

This is a preprint, the final version is subject to change, of the American Mineralogist (MSA)
Cite as Authors (Year) Title. American Mineralogist, in press.
DOI: https://doi.org/10.2138/am-2020-7311

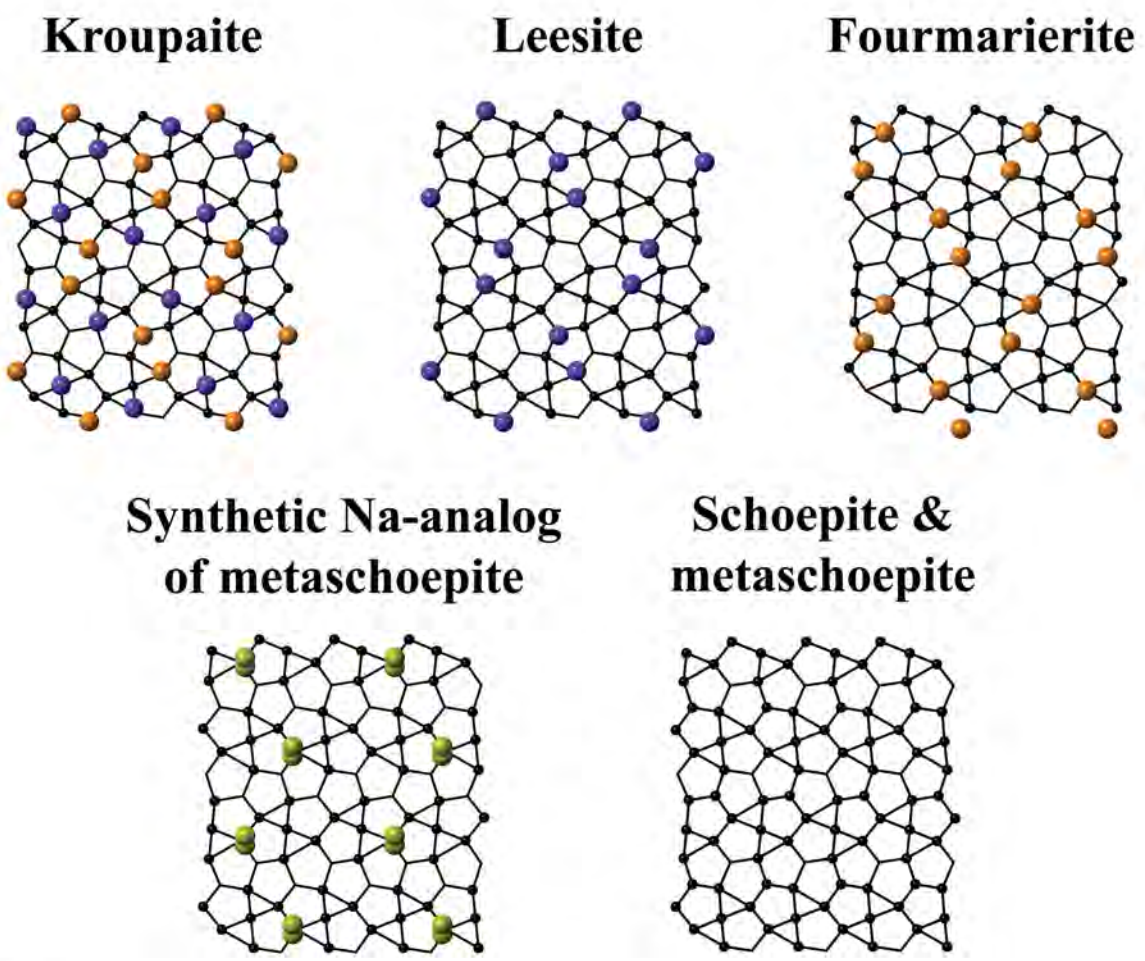

Fig. 5

Always consult and cite the final, published document. See http:/www.minsocam.org or GeoscienceWorld

This is a preprint, the final version is subject to change, of the American Mineralogist (MSA)
Cite as Authors (Year) Title. American Mineralogist, in press.
DOI: https://doi.org/10.2138/am-2020-7311

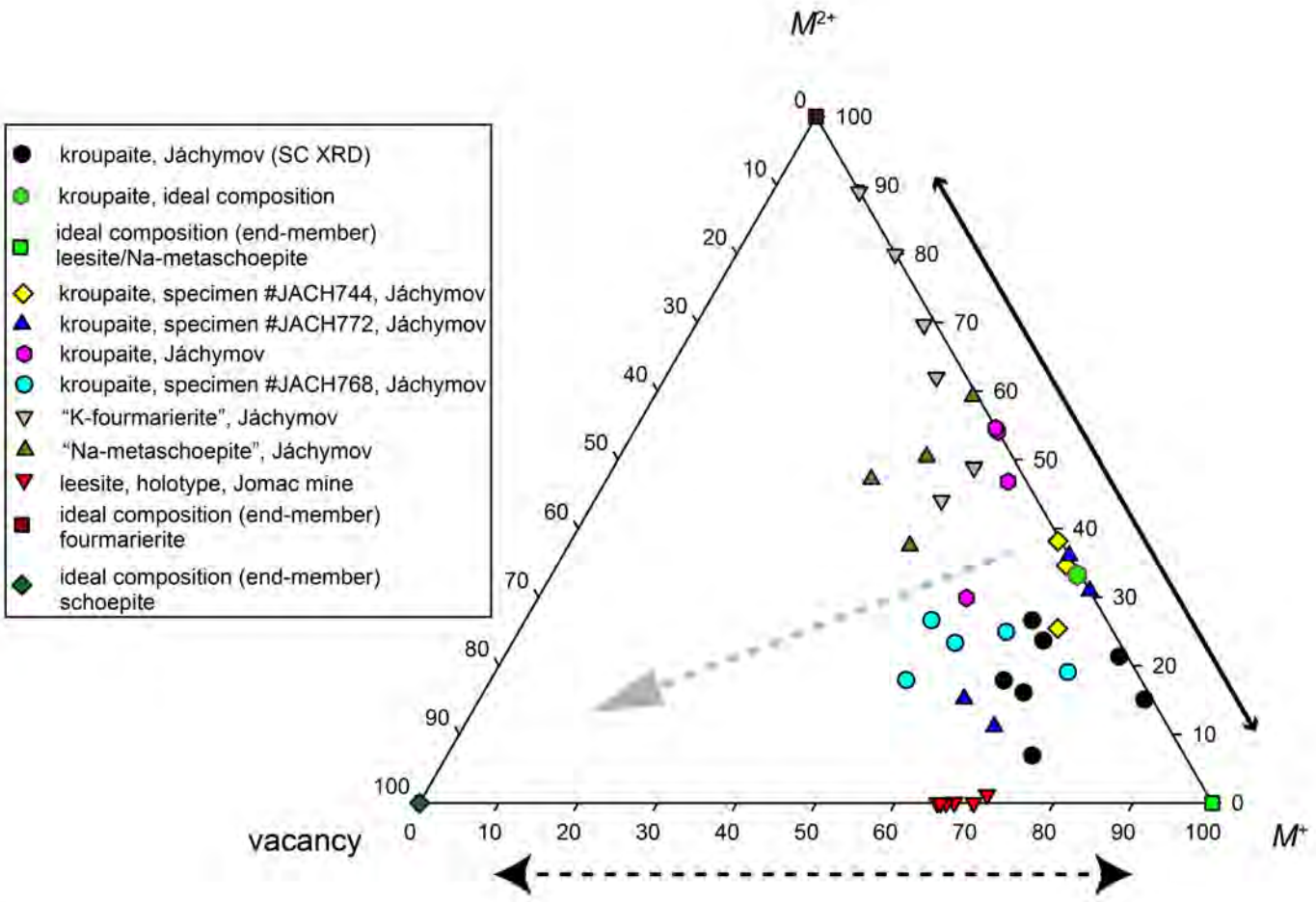

Fig. 6

Always consult and cite the final, published document. See http:/www.minsocam.org or GeoscienceWorld

This is a preprint, the final version is subject to change, of the American Mineralogist (MSA)
Cite as Authors (Year) Title. American Mineralogist, in press.
DOI: https://doi.org/10.2138/am-2020-7311

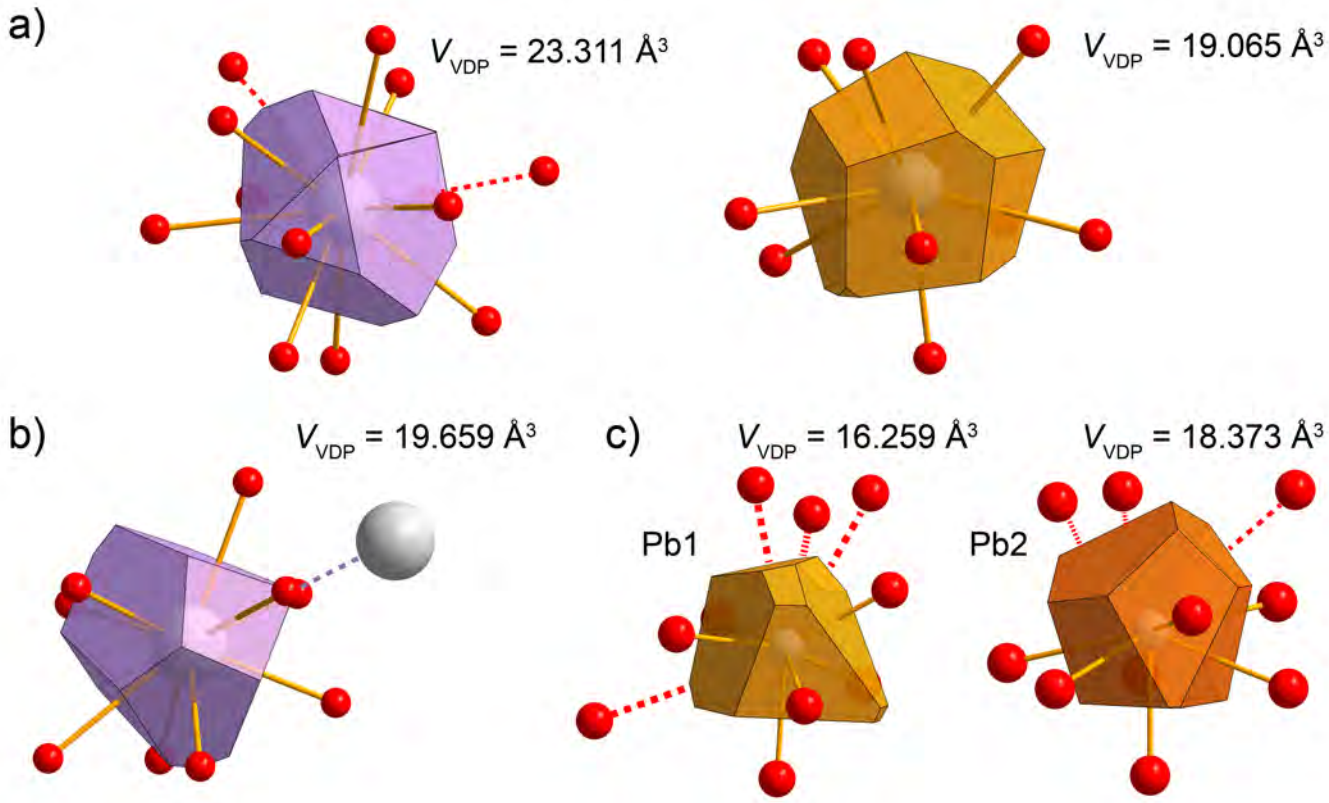

Fig. 7

Always consult and cite the final, published document. See http:/www.minsocam.org or GeoscienceWorld

This is a preprint, the final version is subject to change, of the American Mineralogist (MSA)
Cite as Authors (Year) Title. American Mineralogist, in press.
DOI: https://doi.org/10.2138/am-2020-7311

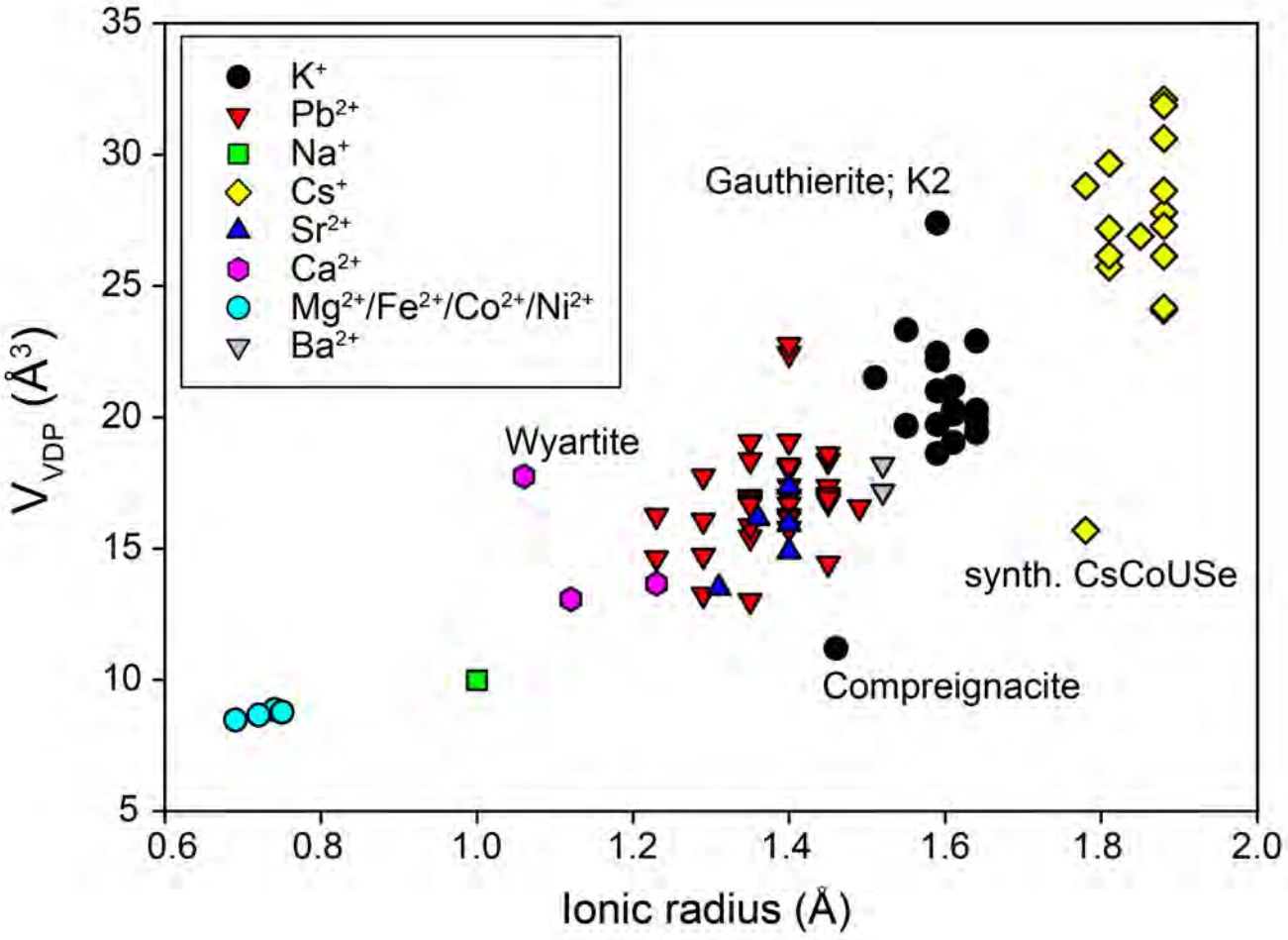

Fig. 8

Always consult and cite the final, published document. See http:/www.minsocam.org or GeoscienceWorld

This is a preprint, the final version is subject to change, of the American Mineralogist (MSA)
Cite as Authors (Year) Title. American Mineralogist, in press.
DOI: https://doi.org/10.2138/am-2020-7311

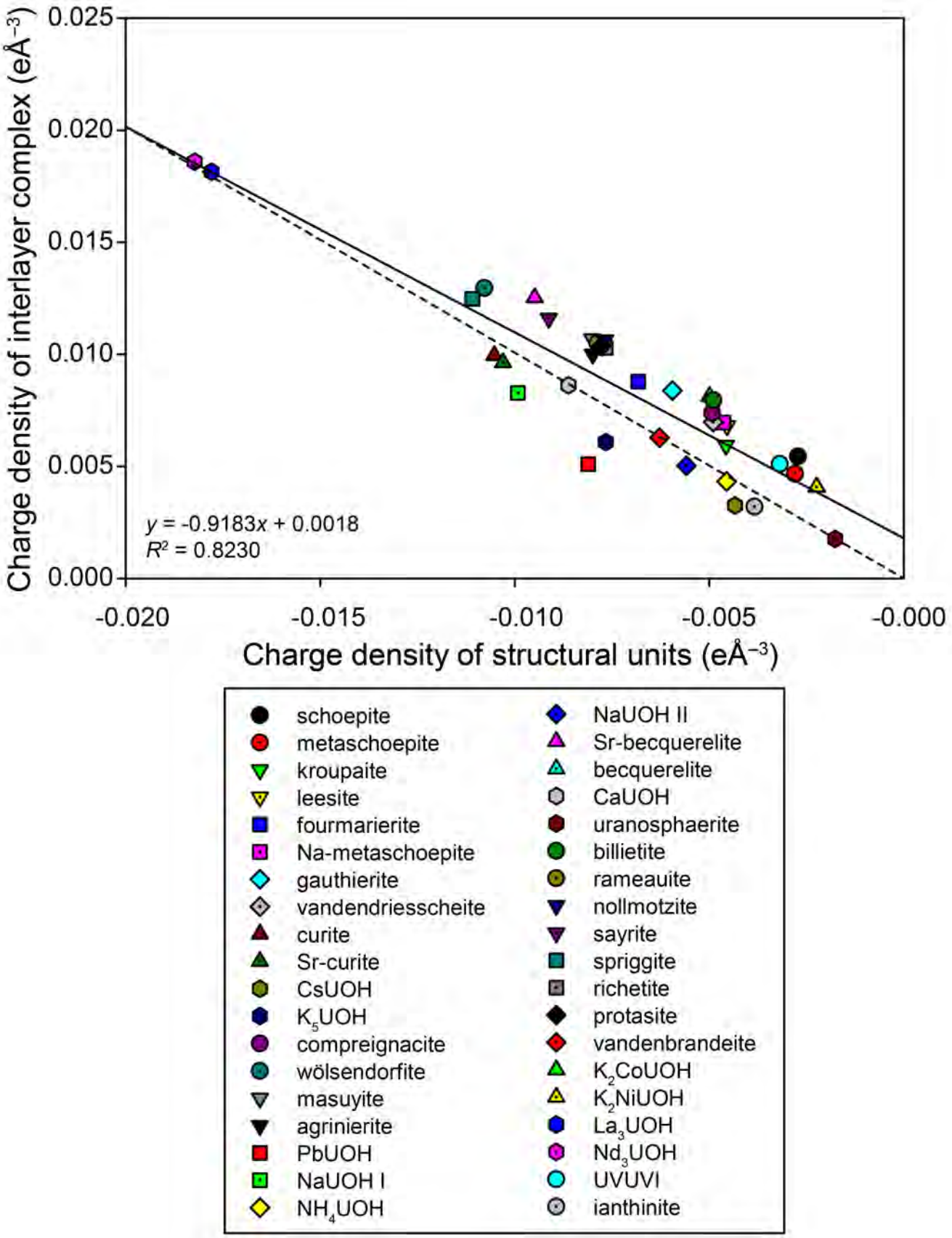

Fig. 9

Always consult and cite the final, published document. See http:/www.minsocam.org or GeoscienceWorld